Pergamon

*Int. J. Heat Mass Transfer.* Vol. 41, No. 12, pp. 1739–1748, 1998

Printed in Great Britain
0017-9310/98 $19.00+0.00

PII: S0017-9310(97)00264-0

# Transition to turbulent flow in curved and straight channels with heat transfer at high Dean numbers

P. M. LIGRANI† and C. R. HEDLUND

Convective Heat Transfer Laboratory, Department of Mechanical Engineering, University of Utah, Salt Lake City, Utah 84112, U.S.A.

(*Received* 15 *May* 1997 *and in final form* 13 *August* 1997)

**Abstract**—Heat transfer in a channel with a straight portion followed by a portion with mild curvature, an aspect ratio of 40, and 0.979 radius ratio is studied at Dean numbers from 700–1100. The effects of curvature, streamwise development, Dean number, and flow tripping are illustrated by the data. Important Nusselt number increases occur due to laminar-to-turbulent transitional phenomena in the straight portion of the channel. Downstream of these increases, flow approaches fully turbulent behavior, and Nusselt numbers collect into families of curves which show weak dependence on Dean number and strong dependence on normalized streamwise distance. © 1998 Elsevier Science Ltd. All rights reserved.

## INTRODUCTION

Heat transfer in channels with transitional and turbulent flows are important for a range of practical applications, including cooling passages in gas turbine blades, internal combustion engine cooling ducts, heat exchangers, fuel grain porting within hybrid rocket motors, and medical treatment of the human cardiovascular system. Straight and curved channels are also interesting because they provide environments to investigate an assortment of transitional phenomena. In straight channels, these phenomena include regions of longitudinally distinct local instability referred to as 'slugs' and 'puffs' of turbulence [1, 2]. In curved channels, transition begins with the development of arrays of counter-rotating Dean vortex pairs which form across the channel span [3, 4, 5]. Whether in straight or curved channels, developing transitional flow events provide the initial conditions for the turbulent flows which follow. The interactions between these transitional phenomena and the subsequently developing turbulent flows can be quite complex, especially when a curved channel segment follows a straight segment, as in the present study.

Only a handful of investigations consider heat transfer in curved channels containing laminar and transitional flows. Of these, Cheng and Akiyama [6] present Nusselt numbers, velocity distributions, and pressure distributions determined from numerical analysis of curved channels with fully developed, laminar forced convection, no buoyancy, and constant heat flux boundary conditions. Mori *et al.* [7] present measured Nusselt numbers from a square channel with laminar, transitional, and turbulent flow conditions, and numerically predicted Nusselt numbers, velocity data, and pressure surveys for fully developed laminar and turbulent channel flows. In another numerical description of curved channel heat transfer, Yee *et al.* [8] predict the streamwise development of Nusselt numbers and secondary motions in curved channels with aspect ratios of 1/3, 1, and 3, and steady, laminar flow with constant wall temperature boundary conditions. Chilukuri and Humphrey [9] numerically predict Nusselt numbers and secondary flows in a curved channel with a square cross-section and buoyancy both assisting and opposing the forced flow. Komiyama [10] presents numerically predicted Nusselt numbers from curved channels with fully developed flows and aspect ratios from 0.8–5, and constant wall heat flux boundary conditions.

Investigations of channels with fully turbulent flow are somewhat more numerous. Recent investigations consider the effects of curvature [11–14], channel aspect ratio and geometry [13–15], ribs and riblets placed along channel walls [15–17], channel Reynolds number [13, 15, 16], duct geometry [14, 15], flow tripping [12], and different surface thermal boundary conditions [11]. Of these investigations, several examine heat transfer behavior in channels with turbulent flows [11, 14–17]. Only Kobayashi *et al.* [11], Joye [14], and Mochizuki *et al.* [16] examine heat transfer in channels with curved sections. Kobayashi *et al.* [12] and Su and Friedrich [13] also investigate turbulent flows in curved channels without heating to illustrate structural characteristics of channel secondary flows. Only Kobayashi *et al.* [11] and Mochizuki *et al.* [16] con-

† Author to whom correspondence should be addressed. Tel.: 801 581 4240. Fax: 801 585 9826. E-mail: ligrani@stress.mech.utah.edu.

**NOMENCLATURE**

| | |
|---|---|
| $d$ | channel thickness |
| $De$ | Dean number $(Ud/v)\sqrt{d/r_i}$ |
| $D_H$ | hydraulic diameter |
| $h$ | heat transfer coefficient, equation (1) |
| $k$ | thermal conductivity |
| $Nu$ | spanwise-averaged Nusselt number, equation (2) |
| $Pr$ | Prandtl number |
| $Re$ | Reynolds number based on channel thickness, $Ud/v$ |
| $Re_{D_H}$ | Reynolds number based on channel hydraulic diameter, $UD_H/v$ |
| $Re_x$ | Reynolds number based on streamwise distance, $Ux/v$ (straight section), $U(x-1.54)/v$ (curved section) |
| $r_i$ | inner radius of channel convex surface |
| $r_o$ | outer radius of channel concave surface |
| $t$ | time-averaged local temperature |
| $t_m$ | mixed-mean temperature |
| $t_w$ | local wall temperature |
| $U$ | bulk mean velocity |
| $x$ | streamwise distance from location where heating begins |
| $X$ | streamwise distance from channel inlet at nozzle exit |
| $Y$ | distance normal from the concave channel surface |
| $Z$ | spanwise distance from channel spanwise centerline. |

Greek symbol

| | |
|---|---|
| $v$ | kinematic viscosity. |

sider the streamwise development of surface heat transfer distributions, channel secondary flows, and temperature distributions in curved channels.

The present study continues efforts begun by Ligrani *et al.* [18], and Hedlund and Ligrani [19]. Ligrani *et al.* [18] examine effects of curvature on measured heat transfer in channels with thermally fully developed, laminar and transitional forced convection. Constant heat flux boundary conditions are applied to the surfaces of the channel, which has an aspect ratio of 40, a bend of 180°, $Pr = 0.71$, and Dean numbers up to 300. The authors indicate that spanwise-averaged Nusselt numbers are always higher on the concave surface than on the convex surface at all streamwise locations in the curved section, except just after curvature begins. Differences just downstream of the beginning of curvature result from initial development of Dean vortex pairs near the concave surface [3–5], and the secondary flows and unsteadiness associated with them [5, 20]. Significant Nusselt number increases on the concave and convex surfaces also occur with $x/d$ for $x/d > 156$ and $De > 150$ due to the twisting secondary instability [5, 21]. Using the same experimental facility, Hedlund and Ligrani [19] examine the effects of upstream transitional flows on curved channel Nusselt numbers at Dean numbers from 300–700. Results suggest that the thermal boundary layers responsible for the Nusselt number variations are dependent upon upstream initial conditions at the inlet of the curved portion of the channel, in addition to transitional disturbances and levels of turbulence intensity very near the measurement location. Local Nusselt number increases from transitional events are believed to be due to local transitional 'slugs' or 'puffs' of turbulence [1, 2]. These cause initial Nusselt number augmentations relative to pure laminar values to be located progressively upstream as the Dean number increases.

In the present work, Nusselt number characteristics at Dean numbers from 700–1100 are investigated, and thus a different range of experimental conditions is covered compared to Ligrani *et al.* [18] or Hedlund and Ligrani [19]. In the flows investigated by Ligrani *et al.* [18], fully developed laminar flow is always present at the inlet of the curved portion of the channel, and transitional events, such as Dean vortex pairs, are contained entirely in the curved portion of the channel. Hedlund and Ligrani [19] describe the effects of transitional events occurring in the straight portion of the channel, upstream of the curved section, on Nusselt number behavior. These transition events provide different initial conditions at the entrance of the curved position of the channel. The present study uses the same channel employed in these two studies, but here, we address Nusselt number behavior as the flows transist to turbulence in the straight portion of the channel, as well as Nusselt number behavior when channel flow is fully turbulent or near-fully turbulent.

Included are descriptions of the influences of streamwise development, varying Dean number, curvature, and flow tripping on local Nusselt number behavior. Of the archival literature known to the authors, only Mori *et al.* [8], Ligrani *et al.* [18] and Hedlund and Ligrani [19] present measured heat transfer data from curved channels with laminar, transitional, and turbulent flows. The present work is thus important as it provides new information regarding effects of complex transitional and turbulent flows on channel heat transfer. As such, the present results provide an important tool for the development of numeric codes for the prediction of these flows.

## EXPERIMENTAL APPARATUS AND PROCEDURES

Details of the experimental apparatus and procedures are given by Ligrani *et al.* [18] and by Hedlund and Ligrani [19]. Brief summaries of these items are also presented here for completeness.

*Channel.* The channel employed here is the same one used by Ligrani *et al.* [18] and Hedlund and Ligrani [19]. Some dimensional details are illustrated in Fig. 1. The channel is instrumented for heat transfer measurements, has a thickness $d$ of 1.27 cm, an aspect ratio of 40, and a radius ratio, $r_i/r_o$, of 0.979. The ratio of shear layer thickness to convex radius of curvature is 0.011 in the curved section, which indicates mild curvature. Air is used as the working fluid.

Just downstream of the channel inlet, the flow is conditioned to reduce spatial non-uniformities using arrays of screens, honeycombs, and a nozzle with a 20 to 1 contraction ratio. Figure 1 shows that the straight section is composed of an initial unheated section 0.57 m long followed by a heated section 1.52 m long. The straight section allows hydrodynamically and thermally fully developed channel flow to develop before entering the curved section at most of the Dean numbers studied [18, 19, 22]. The air then enters a 180° degree curved channel section with convex and concave surface radii of 59.69 and 60.96 cm. Upon exiting the curved section, the flow enters a second straight section with a length of 2.44 m, passing through additional flow management devices and plenums. This serves to isolate the test section from the channel blowers and apparatus for measurement of mass flow rates.

Figure 1 shows four heated sections of the channel walls, denoted CC1, CV1, CC2 and CV2. Each of these segments is instrumented with thermocouples to measure channel surface temperatures, etched foil heaters to heat channel surfaces, and insulation to minimize conduction losses [18, 19, 22]. To facilitate measurement of temperatures on the surface next to the air stream, the interior walls of the heated sections are made of thinner Lexan sheet (0.08 cm) than the unheated portions of the channel. One hundred thermocouples are placed between the heaters and nonflow side of the 0.08 cm Lexan at ten streamwise locations on the convex and concave sides of the channel. These provide sufficient data to calculate spanwise-averaged Nusselt numbers on concave and convex surfaces. Surface temperatures are not measured on the channel end walls. At each location, thermocouples are placed in rows of five. The five thermocouples in each row extend across the channel span a distance of 20.32 cm. Rows of thermocouples on the straight portion of the channel are located at $x/d$ of 12, 36, 60, 84, and 108. This first location corresponds to $X = 0.722$ m. Rows of thermocouples on the curved portion of the channel are located at $x/d$ of 132, 156, 180, 204, and 228.

To determine conductive losses from the heated portions of the channel, 40 additional thermocouples are placed in the insulation located behind the etched foil heaters. These thermocouples are placed in pairs along the channel centerline behind each row of thermocouples to measure the temperature drop through the insulation, and the conduction loss to be determined along all segments of the test section. One additional thermocouple is used to measure the mixed mean temperature at the channel inlet.

*Data acquisition system.* Voltages from the 141 T-type thermocouples are read sequentially using Hewlett-Packard 44422T thermocouple relay multiplexer card assemblies, installed in a HP3497A Data Acqui-

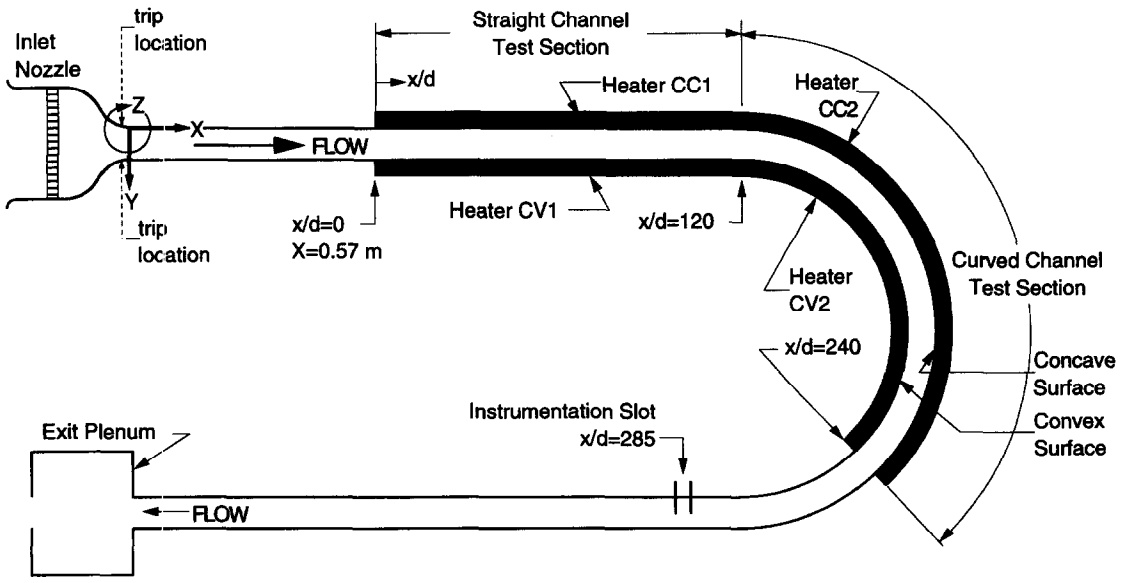


Fig. 1. Channel coordinate system and geometry.

sition/Control Unit and a HP3498A Extender. This system provides thermocouple compensation electronically such that voltages for type $T$ thermocouples are given relative to 0°C. A Hewlett-Packard 9836A computer processes signals from all 141 thermocouples to determine local Nusselt numbers using procedures described below.

*Nusselt number measurement.* After a constant heat flux boundary condition is set, convective heat levels $\dot{q}''_{conv}$ are determined using an equation of the form

$$\dot{q}''_{conv} = ((IV/5) - \dot{q}_{cond})/A$$

where $I$ is the electric current through the heater, $V$ is the voltage drop across the heater, $A$ is the surface area of one segment of the heated test section, and $\dot{q}_{cond}$ is the conductive power lost through the insulation behind each heater segment. The power supplied to each heater segment $IV/5$ is one fifth of the total power supplied to each heater. The local heat transfer coefficient is subsequently given by

$$h = \dot{q}''_{conv}/(t_w - t_m). \quad (1)$$

Wall temperature are determined from thermocouple measured temperatures. These temperatures are corrected to account for the contact resistance between the Lexan and the thermocouples, as well as the conduction through the 0.08 cm thick Lexan sheet separating each thermocouple from the air stream [18, 19]. Local Nusselt number is then given by an equation having the form

$$Nu = hD_H/k. \quad (2)$$

Energy balances are used to determine $t_m$, the local mixed mean temperature at any streamwise channel location in equation (1). The form of the energy balance equation used for this purpose is given by:

$$t_m = t_{m\text{-inlet}} + (\dot{q}''_{conv} b \Delta x)/\dot{m} C_p \quad (3)$$

where $t_{m\text{-inlet}}$ is the mixed mean temperature at the channel inlet, $b$ is the spanwise width of the heated surface, $\Delta x$ is the streamwise distance from the beginning of heating to the streamwise station of interest, $\dot{m}$ is the air mass flow rate, and $C_p$ is air specific heat.

A number of checks of the experimental apparatus and measurement procedures are conducted. These checks focus on Nusselt number spanwise uniformity and overall energy balances. Nusselt number spanwise uniformity is within 0.3 Nusselt number units at higher channel Dean numbers ($>300$), which indicates minimal spanwise conduction losses [18].

Overall energy balance checks are also conducted at Dean numbers less than 300 [18]. These are accomplished by comparing mixed mean temperatures determined at the end of the heated portion of the channel from energy balances to values determined from direct measurements of the local mixed mean temperature just downstream of the heated portion of the channel. In all cases, the two measurements of mixed mean temperature agree within a few percent [18]. The agreement verifies the procedures employed to determine spanwise-averaged Nusselt numbers including conduction energy balances and energy balances to calculate mixed-mean temperatures.

The experimental uncertainty of Nusselt numbers based on a 95% confidence level is ±4%.

## EXPERIMENTAL RESULTS

Nusselt number characteristics at Dean numbers from 700–1080 are discussed in this section in reference to Figs. 2–9. Effects of curvature, streamwise development, Dean number, and flow tripping are described. Correlations of Nusselt number data associated with turbulent flows which are fully developed or near-fully developed are also presented. Because the Reynolds numbers employed are so high, the effects of buoyancy on local Nusselt number behavior are minimal [22, 23]. Dean numbers of 709, 831, 905, and 1084 correspond to $Re$ of 4861, 5697, 6204, and 7432, respectively, and to $Re_{D_H}$ of 9519, 11 157, 12 150, and 14 553, respectively.

*Effects of curvature and streamwise development*

Nusselt numbers are presented as dependent upon normalized streamwise distance in Fig. 2 for Dean numbers of 709, 831, 905, and 1084. Results from the concave and convex surfaces are given at different

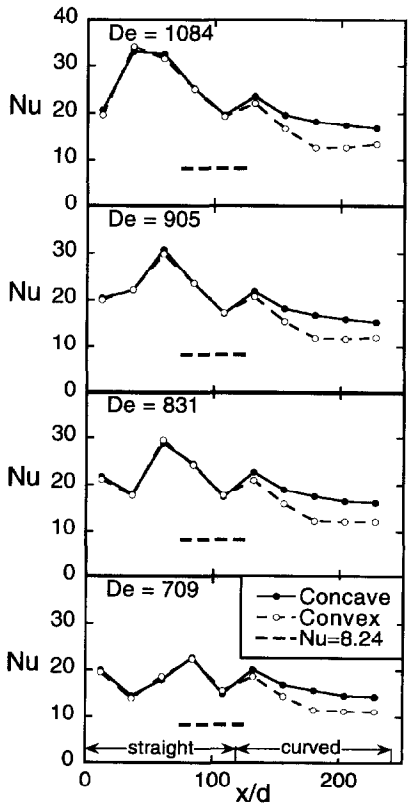


Fig. 2. Forced convection Nusselt numbers as dependent upon $x/d$ for Dean numbers of 709, 831, 905 and 1084.

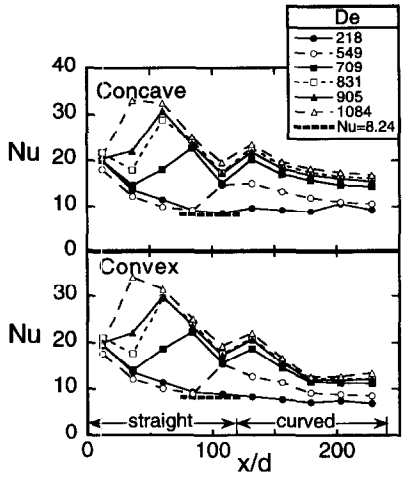


Fig. 3. Forced convection Nusselt numbers as dependent upon $x/d$ for Dean numbers of 218, 549, 709, 831, 905 and 1084 for the concave and convex channel surfaces.

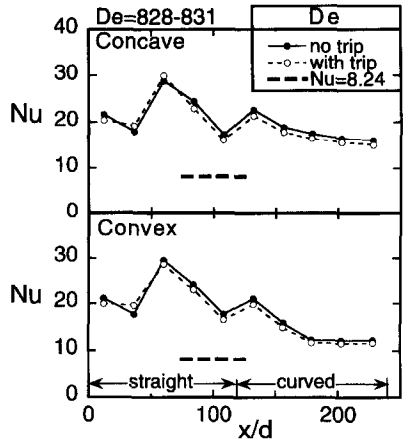


Fig. 5. Effects of tripping on forced convection Nusselt numbers measured at different $x/d$ for Dean numbers from 828–831.

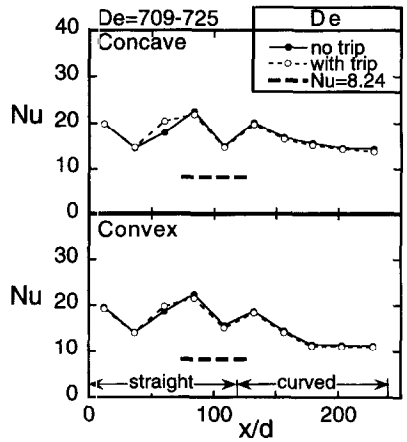


Fig. 4. Effects of tripping on forced convection Nusselt numbers measured at different $x/d$ for Dean numbers from 709–725.

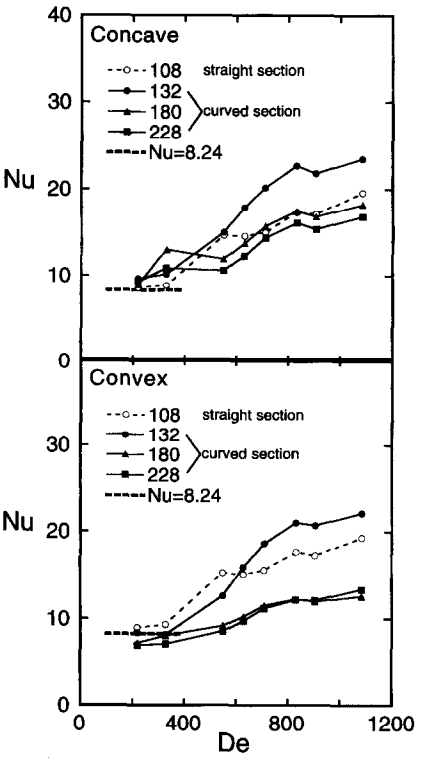


Fig. 6. Comparison of Nusselt numbers in the curved portion of the channel at $x/d$ of 132, 180, and 228 with Nusselt numbers at the downstream end of the straight portion of the channel at $x/d = 108$, as they vary with Dean number.

$x/d$ for each Dean number to illustrate the effects of curvature and streamwise development. Channel curvature begins at $x/d = 120$, as mentioned previously.

Results from the straight portion of the channel in Fig. 2 provide an important check on the experimental data. Nusselt numbers from both the concave and the convex channel surfaces are the same at similar $x/d$ and $De$ for all four Dean numbers. This agreement evidences consistent measurement procedures, and two-dimensional, time-averaged velocity and thermal fields. This is also important because the flow conditions at the exit of the straight channel provide the thermal and velocity inlet conditions for the curved portion of the channel. The Nusselt number predicted for fully developed laminar flow between infinite parallel flat plates is $Nu = 8.24$ and is also indicated on Fig. 2. $Nu$ magnitudes near the downstream end of the straight portion of the channel at $x/d$ just less than 120 at all four Dean numbers are greater than 8.24 in Fig. 2, which is expected as the channel experiences transitional events prior to $x/d = 120$ at all four Dean numbers. The transitional events leading to turbulent

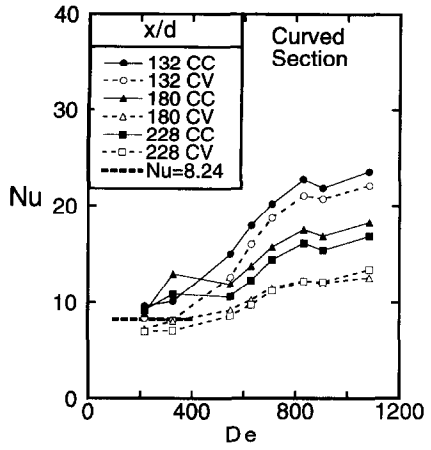


Fig. 7. Comparison of Nusselt numbers from the concave surface of the channel with Nusselt numbers from the convex surface of the channel at $x/d$ of 132, 180 and 228 as they vary with Dean number.

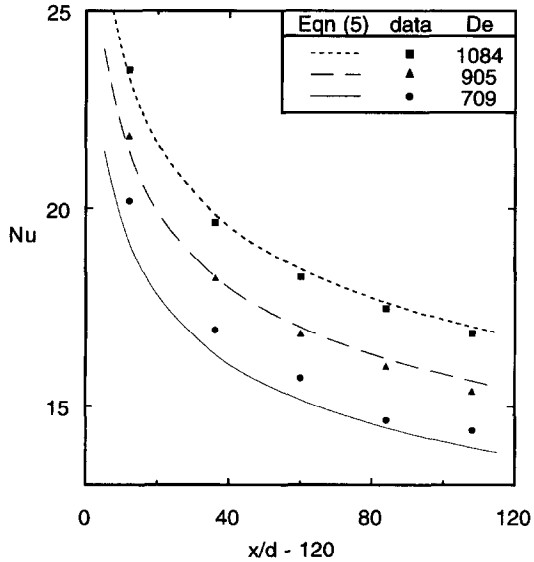


Fig. 8. Fully turbulent or near-fully turbulent concave surface Nusselt numbers as dependent upon $x/d$ at Dean numbers of 709, 905 and 1084, including the Nusselt number correlation for fully turbulent flow as a function of $x/d$ and Reynolds number based on hydraulic diameter.

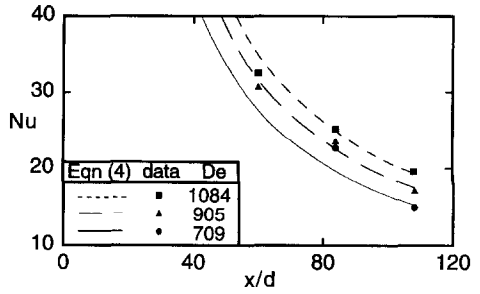


Fig. 9. Fully turbulent or near-fully turbulent straight surface Nusselt numbers as dependent upon $x/d$ at Dean numbers of 709, 905 and 1084, including the Nusselt number correlation for fully turbulent flow as a function of $x/d$ and Reynolds number based on hydraulic diameter.

flow always occur in the straight portion of the channel at all four Dean numbers, and the location of the onset of these transitional events moves progressively upstream as the Dean number increases.

In the curved portion of the channel ($x/d$ from 120–240), Nusselt numbers measured on the concave surface are consistently higher than values measured on the convex surface in Fig. 2 for all four Dean numbers. This indicates Dean vortex pairs are not only present in the channel at Dean numbers from 709–1084, but that they also strongly influence thermal flow field behavior. As for the results at lower Dean numbers [18, 19], differences in Nusselt numbers between the concave and convex surfaces are about the same for the different Dean numbers when compared at the same $x/d$ in spite of: (i) different transitional and turbulent flow events upstream, and (ii) different thermal and velocity conditions present at $x/d = 120$, at the inlet of the curved portion of the channel.

Nusselt numbers on the concave surface are higher than Nusselt numbers on the convex surface measured at the same streamwise location because of more intense secondary flows and greater local unsteadiness due to motion within and very near to the Dean vortices near the concave surface. Kobayashi *et al.* [11, 12] and Su and Friedrich [13] also provide evidence of important secondary flow motions from vortices in fully turbulent channel flows. In Kobayashi *et al.* [11], these are evidenced by different streamwise development and different magnitudes of wall shear stress and wall heat flux measured on convex and concave channel surfaces. Magnitudes of velocity temperature cross-correlation coefficients, triple temperature correlations, and the skewness and flatness of velocity and temperature fluctuations also illustrate differences in flow structure due to vortices in flows near concave and convex surfaces [11]. In a companion paper, Kobayashi *et al.* [12] provide statistical descriptions of large-scale eddies near the concave surface and small-scale eddies near the convex surface from power spectra of velocity fluctuations and spanwise correlations of velocity fluctuations. The large-scale eddies augment magnitudes of turbulent stresses and provide mechanisms to increase momentum transport, thermal transport, and local Nusselt numbers on and near concave surfaces. According to the authors, the large-scale eddies are not as steady as the turbulent Taylor–Gortler vortices since they 'sway' in the spanwise direction and their spatial extents vary irregularly with time [12].

*Effects of Dean number*

The results from Fig. 2 are again plotted in Fig. 3 along with two additional Nusselt number data sets for $De = 218$ and $De = 549$ [18, 19]. In the top portion

of Fig. 3, data measured on the concave surface for all Dean numbers are plotted together. In the bottom portion of Fig. 3, the convex surface data for all Dean numbers are plotted together.

The Nusselt number data in Fig. 3 for $De = 218$ represent pure laminar behavior in the straight portion of the channel ($0 < x/d < 120$). Here, $Nu$ values first decrease with $x/d$ and then become approximately constant with $x/d$ at $x/d = 80$–120, where values are close to 8.24. This Nusselt number is the expected value for fully developed flow in a straight channel with infinite aspect ratio and constant heat flux boundary conditions. As mentioned earlier, Dean vortex pairs form soon after the flow enters the channel at $x/d$ just greater than 120. Near the downstream end of the channel, the Dean vortex pairs at $De = 218$ then develop the twisting secondary instability [21], which causes Nusselt numbers from the concave surface to increase as $x/d$ increases from 180–204. Convex surface Nusselt numbers, on the other hand, are relatively unaffected by the twisting instability in the vortices at this experimental condition.

Figure 3 shows that additional important Nusselt number increases with $x/d$ occur at smaller $x/d$ as the Dean number increases from 549–1084. In contrast to the Nusselt number variations from twisting, these changes occur in the straight portion of the channel and affect both channel surfaces. At $De = 709$, this local Nusselt number increase occurs as $x/d$ increases from 36–84, at $De = 831$, this local Nusselt number increase occurs as $x/d$ increases from 36–60, at $De = 905$, this local Nusselt number increase occurs as $x/d$ increases from 12–60, and at $De = 1084$, this increase occurs at $x/d$ up to 36. Each of these is due to transitional events, most likely local 'slugs' of turbulence which originate from instability waves of entry region boundary layers [1, 2]. These cause initial heat transfer coefficient augmentations relative to pure laminar values to be located progressively upstream (at smaller $x/d$) as the Dean number increases.

Figure 3 also shows that Nusselt numbers on both the concave and convex channel surfaces at $De = 709$ are significantly higher than values measured at $De = 218$ and at $De = 549$, except for $x/d < 36$. This Nusselt trend continues at $x/d < 84$ as the Dean number increases even further to $De = 831, 905$, and 1084, since Nusselt numbers continue to increase with $De$ at each $x/d$ within this range. Another interesting feature of the Nusselt number data in Fig. 3 is the trend followed by the results measured in the straight portion of the channel ($0 < x/d < 120$). For each $De$ from 709–1084, Nusselt numbers just downstream of the transition region (i.e $x/d > 84$ for $De = 709$, $x/d > 60$ for $De = 831$, 905, and 1084) follow a single family of curves. The curves in the family show weak dependence on Dean number, and each curve in the family has about the same slope when compared at the same $x/d$. The uniform $x/d$ dependence of the curves in the family at $x/d$ from 60–84–120 thus represents Nusselt number behavior for both channel surfaces in a near-fully turbulent straight channel with developing thermal boundary layers.

As each of these flows ($De = 709$, 831, 905 and 1084) progresses through the curved portion of the channel ($120 < x/d < 240$), concave side Nusselt numbers again follow a single family of curves. Here, Nusselt numbers again show uniform dependence on $x/d$ when compared at the same $x/d$ at all $De$ in this range, and weak dependence on Dean number at each $x/d$. All of the curves thus have about the same slope when compared at the same $x/d$. In this case, the family of curves represents Nusselt number behavior on the concave surface in a fully turbulent (or near-fully turbulent) curved channel with thermal boundary layers which are close to being fully developed.

Nusselt numbers measured at $De$ equal to 709, 831, 905, and 1084 on the convex side of the channel also roughly collect into a single family of curves, however, these data show different slopes at different Dean numbers when compared to the same $x/d$. Two distinctly different types of convex surface behavior are apparent in Fig. 3 for this range of Dean numbers, which are located at $120 \leqslant x/d < 180$, and $180 \leqslant x/d < 228$. In the upstream portion of the curved section of the channel at $120 < x/d < 180$, the convex side Nusselt number variation at each $De$ seem to converge as they descend steeply and $x/d$ increases. As $x/d$ then increases from 180, convex side Nusselt numbers remain approximately constant with $x/d$ when $De$ is 709 and 831. Nusselt numbers then increase with increasing $x/d$ when $De$ is 905 and 1084. Convex side Nusselt numbers at different Dean numbers thus diverge slightly from each other over as $x/d$ increases for $x/d > 180$.

In the straight portion of the channel, turbulent Nusselt numbers at $De = 905$ are represented by dependence on $(x/d)^{-1.0}$ or $(Re_x)^{-1.0}$. In the curved portion of the channel, turbulent Nusselt numbers from the concave surface of the channel at $De = 905$ are represented by dependence upon $(x/d-120)^{-0.140}$ or $(Re_x)^{-0.140}$. Thus Nusselt numbers from the concave surface decrease significantly more slowly with $x/d$ than ones measured in the straight portion of the channel. This is because the thermal boundary layers in the straight portion of the channel are developing, whereas the layers in the curved portion are close to being fully developed. Similar Nusselt number dependence on $x/d$ and $Re_x$ is valid for Nusselt number data at other Dean numbers, provided the flow in the channel is locally fully turbulent or approaching fully turbulent behavior. No attempt is made to determine turbulent Nusselt number dependence on $x/d$ and $Re_x$ for the convex surface since those data have different slopes at different $De$ when compared at the same $x/d$.

*Effects of tripping the flow*

All experimental data presented thus far were obtained with no trips placed in the channel inlet. Here, Nusselt number results are described for

$De$ = 709–725 and $De$ = 828–831 which are obtained with 2 mm trips placed across the entire span of both convex and concave surfaces near the downsteam end of the inlet nozzle. These data are compared to results obtained with no trips to provide indications of events altered by the presence of near wall disturbances initiated at the inlet of the straight portion of the channel.

Nusselt number distributions, obtained with and without trips, are presented in Figs. 4 and 5 for $De$ = 709–725 and $De$ = 828–831, respectively. In both cases, the trips have little effect on local Nusselt number behavior, except near $x/d = 60$ for $De$ = 709–725 and near $x/d = 36$ for $De$ = 828–831, where the trips produce slightly higher local $Nu$ values. Much larger changes of the local Nusselt number are produced by the trips at lower Dean numbers [19]. The quantitatively small effects of the trips for $De$ = 709–831 suggests that transitional events at these locations are already so strong that the disturbances from the trips produce little additional effects. The local Nusselt number increases in Figs. 4 and 5 also may suggest an increase in the frequency and/or intensity of localized 'puffs' of turbulence [1, 2, 19].

*Overall data trends with Dean number*

Results which illustrate overall data trends with Dean number are presented in Figs. 6 and 7.

In the upper portion of Fig. 6, concave surface Nusselt numbers from the curved portion of the channel, measured at different streamwise locations at $x/d$ = 132, 180 and 228, are compared to Nusselt numbers near the end of the straight portion of the channel, at $x/d = 108$. The lower portion of Fig. 6 shows Nusselt numbers from the corresponding streamwise locations on the convex surface for comparison to Nusselt numbers at $x/d = 108$. Note that concave and convex labels are used for the two parts of Fig. 6, including the $x/d = 108$ location, even though this corresponds to the downstream portion of the straight portion of the channel.

Figure 6 gives Nusselt numbers at the downstream end of the straight portion of the channel ($x/d = 108$) from both channel surfaces which are quite close to $Nu = 8.24$ at Dean numbers from 200–400. As $De$ increases, Nusselt numbers for $x/d = 108$ also increase to approach fully turbulent or near-fully turbulent magnitudes when the Dean number becomes greater than about 600. This corresponds to a Reynolds number based on channel hydraulic diameter, $Re_{D_H}$, of approximately 8000. With the exception of $Nu$ values measured on the concave and convex surfaces near the beginning of curvature of $x/d = 132$, most of the Nusselt numbers from the curved surfaces in Fig. 6 are then less than values measured near the end of the straight surfaces when compared to the same $De$. Nusselt numbers from all curved section locations increase with Dean number, except for values measured on the concave surface at $De$ from 400–600 and $x/d$ of 180 and 228.

Curved surface results from Fig. 6 are plotted again in Fig. 7 so that a direct comparison of Nusselt numbers from the concave and convex surface can be made. In this figure, CC denotes results measured on the concave surface, and CV denotes results measured on the convex surface. The strong dependence of Nusselt numbers on Dean number and normalized streamwise location is evident from the figure. Nusselt numbers, especially ones measured in the convex surface, are near 8.24 at Dean numbers from 200–400. Differences between concave and convex Nusselt numbers are evident near the beginning of curvature at $x/d = 132$ which become larger as the Dean number increases. As the Dean number then becomes greater than 200–400, Nusselt numbers also generally increase, with the exception of data at $De$ from 400–600 and $x/d$ of 180 and 228. As this happens, the flow in the curved channel proceeds through a sequence of transitional events, including the development of arrays of Dean vortex pairs across the channel cross section [3–5, 24–26], splitting and merging of vortex pairs [5, 20, 24, 27], vortex pair undulations [21], and vortex pair twisting [21, 24, 26]. Twisting then leads to local regions of turbulence and then to fully turbulent flow [21]. Other transitional events [1, 2] in the upstream straight portion of the channel result in turbulent flow or near-fully turbulent flow at $x/d = 120$ at the entrance of the curved portion of the channel when Dean numbers become greater than about 600.

As the Dean number increases beyond this value, Nusselt number data in Fig. 7 then continue to show important variations with Dean number and $x/d$. These are believed to be mostly due to the continued presence of arrays of Dean vortex pairs in the fully turbulent curved channel, but are probably also influenced by different transition events originating in the straight portion of the channel located just upstream. A slight Nusselt number decrease (which is within experimental uncertainty ranges) is also evident in Fig. 7 as the Dean number increases from 831–905. Thus, Nusselt numbers show somewhat smaller variations with Dean number as the Dean number increases above 800.

Nusselt number correlations for turbulent (or near-fully turbulent) channel flows, which express Nusselt number dependence on Reynolds number based on channel hydraulic diameter and normalized streamwise distance, are given by

$$Nu = 10.35 \cdot Re_{D_H}^{0.554} \cdot (x/d)^{-1.0} \tag{4}$$

for the straight portion of the channel, and

$$Nu = 0.386 \cdot Re_{D_H}^{0.464} \cdot (x/d - 120)^{-0.14} \tag{5}$$

for the concave surface of the curved portion of the channel, respectively. Figure 8 shows that equation (5) provides a good match to the family of data associated with the concave channel surface when the channel flow is fully turbulent or near-fully turbulent at $De$ of

709, 905, and 1084. Figure 9 shows that equation (4) generally matches the family of data associated with the straight portion of the channel when the channel flow is fully turbulent or near to fully turbulent behavior for the same Dean numbers. Small differences between the data and equation (4) are present because the change from transitional to turbulent flow does not occur abruptly at a single $x/d$ location. The power law dependence on Reynolds number changes slightly at the different fully turbulent $Re_{D_H}$ and $De$ considered. The values given by equations (4) and (5) thus represent the best fits to all of our measured turbulent and near-fully turbulent Nusselt number data.

## SUMMARY AND CONCLUSIONS

Heat transfer in a channel with a straight portion followed by a portion with mild curvature, an aspect ratio of 40, and 0.979 radius ratio is studied at Dean numbers from 700–1100. The effects of curvature, streamwise development, Dean number, and flow tripping are illustrated by the data.

At each Dean number investigated from 709–1084, important Nusselt number increases with $x/d$ occur in the straight portion of the channel due to laminar-to-turbulent transitional phenomena. Downstream of these increases ($x/d > 84$ for $De = 709$, $x/d > 60$ for $De = 831$, 905, and 1084), flow is turbulent or near-fully turbulent, and Nusselt numbers in the straight portion of the channel at $x/d$ from 0–120 collect into a single family of curves. Nusselt number variations in the family show weak dependence on Dean number and strong dependence on normalized streamwise distance. Each curve in the family has about the same slope when compared at the same $x/d$. The uniform $x/d$ dependence of the curves in the family at $x/d$ from 60–84 to 120 thus represents Nusselt number behavior for both channel surfaces in a near-fully turbulent straight channel with developing thermal boundary layers.

As each of these flows ($De = 709$, 831, 905, and 1084) progresses through the curved portion of the channel ($120 < x/d < 240$). Nusselt number variations with $x/d$ from the concave surface again follow a single family of curves. Each curve again shows approximately the same dependence on $x/d$ when compared at the same $x/d$ at each of these Dean numbers. These Nusselt number data thus represent fully turbulent or near-fully turbulent concave curved channel flow with thermal boundary layers which are close to being fully developed. Nusselt numbers associated with flows experiencing transition in the curved portion of the channel [18, 19] thus show different dependence on $De$ and $x/d$ compared to Nusselt numbers measured with turbulent flow in the curved portion of the channel. In the former case, Nusselt numbers change magnitudes significantly at a particular $x/d$ as the location and/or character of upstream transition events change with $De$, whereas near-fully turbulent Nusselt numbers do not.

Nusselt numbers measured on the concave surface in this portion of the channel are significantly higher than values measured on the convex surface when compared at the same $x/d$. Thus, Dean vortex pairs are not only present in the channel at these Dean numbers, but they also strongly influence thermal flow field behavior, even when the curved channel flow is fully turbulent (or near-fully turbulent). This vortex-dependent behavior and the family dependence of fully turbulent Nusselt numbers on $x/d$ and $De$ occur in spite of: (i) different characteristics and locations of transitional events occurring upstream at the same $De$ in the straight portion of the channel, and (ii) different initial conditions characterized by thermal and velocity profiles at $x/d = 120$ at the inlet of the curved portion of the channel.

*Acknowledgements*—This work was sponsored by the Propulsion Directorate, U.S. Army Aviation Research and Technology Activity-AVSCOM, through NASA-Defense Purchase Request C-30030-P. The program monitor was Mr Kestutis Civinskas.

## REFERENCES

1. Ligrani, P. M., Subramanian, C. S., Coumes, T. M., Greco, F. J., Koth, H. and Longest, J. M., Study of the imposition of bulk flow pulsations on plane channel flow at moderate Stokes numbers. *Experimental Thermal and Fluid Science*, 1992, **5**, 145–161.
2. Stettler, J. C. and Hussain, A. K. M. F., On transition of the pulsatile pipe flow. *Journal of Fluid Mechanics*, 1986, **170**, 169–197.
3. Dean, W. R., Fluid motion in a curved channel. *Proceedings of the Royal Society of London, Series A*, 1928, **121**, 402–420.
4. Brewster, D. B., Grosberg, P. and Nissan, A. H., The stability of viscous flow between horizontal concentric cylinders. *Proceedings of the Royal Society of London, Series A*, 1959, **251**, 76–91.
5. Ligrani, P. M. and Niver, R. D., Flow visualization of Dean vortices in a curved channel with 40 to 1 aspect ratio. *Physics of Fluids*, 1988, **31**, 3605–3617.
6. Cheng, K. C. and Akiyama, M., Laminar forced convection heat transfer in curved rectangular channels. *International Journal of Heat and Mass Transfer*, 1970, **13**, 471–490.
7. Mori, Y., Uchida, Y. and Ukon, T., Forced convective heat transfer in a curved channel with a square cross section. *International Journal of Heat and Mass Transfer*, 1971, **14**, 1787–1805.
8. Yee, G., Chilukuri, R. and Humphrey, J. A. C., Developing flow and heat transfer in strongly curved ducts of rectangular cross section. *ASME Transactions, Journal of Heat Transfer*, 1980, **102**(2), 285–291.
9. Chilukuri, R. and Humphrey, J. A. C., Numerical computation of buoyancy induced recirculation in curved square duct laminar flow. *International Journal of Heat and Mass Transfer*, 1981, **24**, 305–314.
10. Komiyama, Y., Laminar forced convection heat transfer in curved channels of rectangular cross-section. *Transactions of the Japan Society of Mechanical Engineers B*, 1984, **50**(450), 424–434.
11. Kobayashi, M., Maekawa, H., Takano, T. and Kobayashi, M., Experimental study of turbulent heat transfer in a two-dimensional curved channel (time-mean temperature and multiple temperature/velocity correlations

in the entrance section). *JSME International Journal, Series B: Fluids an Thermal Engrg.*, 1994, **37**(3), 545–553.
12. Kobayashi, M., Maekawa, H., Shimizu, Y. and Uchiyama, K., Experimental study on turbulent flow in two-dimensional curved channel (space/time correlations and spectra of velocity fluctuations). *JSME International Journal, Series B: Fluids and Thermal Engrg.*, 1992, **37**(1), 38–46.
13. Su, M. D. and Friedrich, R., Numerical simulation of fully developed flow in a curved duct of rectangular cross section. *International Journal of Heat and Mass Transfer*, 1994, **37**(8), 1257–1268.
14. Joye, D. D., Optimum aspect ratio for heat transfer enhancement in curved rectangular channels. *Heat Transfer Engrg.*, 1994, **15**(2), 32–38.
15. Lorenz, S., Nachtigall, C. and Leiner, W., Permanent three-dimensional patterns in turbulent flows with essentially two-dimensional wall configurations. *International Journal of Heat and Mass Transfer*, 1996, **39**(2), 373–382.
16. Mochizuki, S., Murata, A. and Fukunaga, M., Effects of rib arrangements on pressure drop and heat transfer in a rib-roughened channel with a sharp 180 degree turn. ASME Paper No. 95-CTP-3, 1995.
17. Fusegi, T., Turbulent flow calculations of mixed convection in a periodically ribbed channel. *Journal of Enhanced Heat Transfer*, 1995, **2**(4), 295–305.
18. Ligrani, P. M., Choi, S., Schallert, A. R. and Skogerboe, P. E., Effects of Dean vortex pairs on surface heat transfer in curved channel flow. *International Journal of Heat and Mass Transfer*, 1996, **39**, 1, 27–37.
19. Hedlund, C. R. and Ligrani, P. M., Heat transfer in curved and straight channels with transitional flow. *International Journal of Heat and Mass Transfer*, 1998, **41**(3), 563–573.
20. Ligrani, P. M., Longest, J. E., Kendall, M. R. and Fields, W. A., Splitting, merging and spanwise wavenumber selection of Dean vortex pairs. *Experiments in Fluids*, 1994, **18**(1), 41–58.
21. Ligrani, P. M., Finlay, W. H., Fields, W. A., Fuqua, S. J. and Subramanian, C. S., Features of wavy vortices in a curved channel from experimental and numerical studies. *Physics of Fluids A*, 1992, **4**(4), 695–709.
22. Hedlund, C. R., Effects of transition to turbulence and Dean vortex pairs on surface heat transfer in curved and straight channels at moderate and high Dean numbres. M.S. thesis, University of Utah, Salt Lake City, Utah, 1996.
23. Ligrani, P. M. and Choi, S., Mixed convection in straight and curved channels with buoyancy orthogonal to the forced flow. *International Journal of Heat and Mass Transfer*, 1996, **39**, 12, 2473–2484.
24. Matsson, O. J. E. and Alfredsson, P. H., Curvature- and rotation-induced instabilities in channel flow. *Journal of Fluid Mechanics*, 1990, **210**, 537–563.
25. Bottaro, A., Matsson, O. J. E. and Alfredsson, P. H., Numerical and experimental results for developing channel flow. *Physics of Fluids A*, 1991, **3**, 1473–1476.
26. Matsson, O. J. E. and Alfredsson, P. H., Experiments on instabilities in curved channel flow. *Physics of Fluids A*, 1992, **4**, 1666–1676.
27. Bottaro, A., On longitudinal vortices in curved channel flow. *Journal of Fluid Mechanics*, 1993, **251**, 627–660.